IOSR Journal of Applied Geology and Geophysics (IOSR-JAGG)
e-ISSN: 2321–0990, p-ISSN: 2321–0982.Volume 6, Issue 3 Ver. III (May. – June. 2018), PP 09-17
www.iosrjournals.org

Pore Systems Analysis of Posidonia and Wealden Shales of Lower Saxony Basin, Germany

*M. Bukar[1], F. A. Rufai[2], A. Y. Kuku[1], M. Halilu[2] and B. Shettima[1]
[1]*Geology Department, University of Maiduguri, Nigeria*
[2] *Geology Department, Modibbo Adama University of Technology Yola, Nigeria*
Corresponding Author: M. Bukar

Abstract: *As the global demand of natural gas increases, exploration for source of natural gas also increased in recent times, shale is being considered as gas storage facility. The aim of this research is to examine and characterise pores between organic and inorganic mineral grains from both Posidonia and Wealden shales of the lower Saxony Basin, Germany using the nanometer-scaled pore systems. This is to ascertain their gas storage capabilities as well as permeability pathways and to also compare mercury injection data with the measured porosity. Focused ion beam, broad ion beam, scanning electron microscope imaging and mercury intrusion porosimetry were used to study the porosity of these shale samples. Qualitative and quantitative description of microstructures and pores were carried out using Jmicrovision v.1.27 computer software. Pore system is found to be dominated by angular and ellipsoidal interparticle pores connected by narrow tube like pore-throats and subordinate poorly connected ellipsoidal intraparticle pores and no organic matter pores were identified probably due to immature nature of the samples. Some artefact pseudo-pores were introduced into the samples during sample preparations. Mercury intrusion porosimetry gave porosity of 6.5% and 5.9% which are higher than measured porosity of 2.5% and 0.5% for Posidonia and Wealden shales respectively. These pores could be the possible storage for natural gas accumulation when generated.*

Keywords: *Broad ion beam (BIB), Focused ion beam (FIB), nanometre-scale, Posidonia, Wealden.*

Date of Submission: 02-06-2018 Date of acceptance: 18-06-2018

I. Introduction

The ability to economically produce gas and oils from rocks that have traditionally been considered both as source and seals has forced a paradigm shift in our understanding of the pore structure of low-permeability rocks. Understanding the pore system of these rocks has been hindered by our lack of tools to investigate their pore structure (Gareth et al., 2011). Porosity and permeability are two parameters to consider in oil and gas production. Porosity is the fraction or void (empty) spaces in a rock, this void spaces can be between grains or within cracks or cavity of rocks. The void spaces have the ability to store oil, gas or water. Permeability is a measure of ease with which a fluid or gas can move through a porous rock. Shale, an argillaceous material is characterized by its low macro porosity and permeability; it takes a lot of pressure to squeeze fluid through a rock that has low permeability.

Shale research has recently gained popularity as a future source of gas storage. Its significance led to the scientific studies/investigations of several shale systems. Recent studies showed that a pore network may have one dominant pore type or a complex combination. Mudstones from the Barnett Shale for example have a pore network dominated by organic-matter intraparticle pores, whereas the Pearsall Shale appears to have a pore network dominated by interparticle and intraparticle pores (Loucks et al., 2011). Imaging of pore space in fine grained geological materials is a rapidly developing field since ion milling had shown to produce smooth and damage free surfaces (Holzer et al., 2007, 2010; Loucks et al., 2009). Measurement of porosity depends strongly on the method used, as different methods detect different classes of pores. Pores in mudrocks are not easily identified using conventional sample-preparation methods. This is due to the fact that artefacts are difficult to differentiate from real/true pores. Hence, to image pores accurately new approaches have been implemented (Reed and Loucks, 2007). With that pores can be recognized as small as 5nm. Loucks et al, (2009) stated that micropores are also associated with diagenetic minerals during its transformation to rock. These minerals may be quartz or pyrite which will eventually fill the moulds left by fossils such as algal spore and forming casts. Organic-matter pores and interparticle pores have better probabilities that may be connected and form a permeable pathway than isolated intraparticle pores (Loucks et al., 2011).

Loucks et al., (2009) and Sondergeld et al., (2010) documented that pores identified using SEM and FESEM may really be remnant depressions of grains that were artificially plucked during sample preparation and polishing caused by mineral hardness. The artificially made pores are circular or ellipsoidal in shape and the

holes extend only a few nanometres in depth, revealing the surrounding matrix at their base. Whereas the natural made pores are irregular in shape (except sponge spicules dissolution pores) and extend deeper into the matrix which is clearly different from the holes formed by grain plucking.

Samples from Posidonia and Wealden shales of the lower Saxony basin (Fig. 1) were analysed for pore system characterization. The aim of this research is to characterize pore types, quantify pore statistics and compare measured and mercury injection porosity of the shale samples.

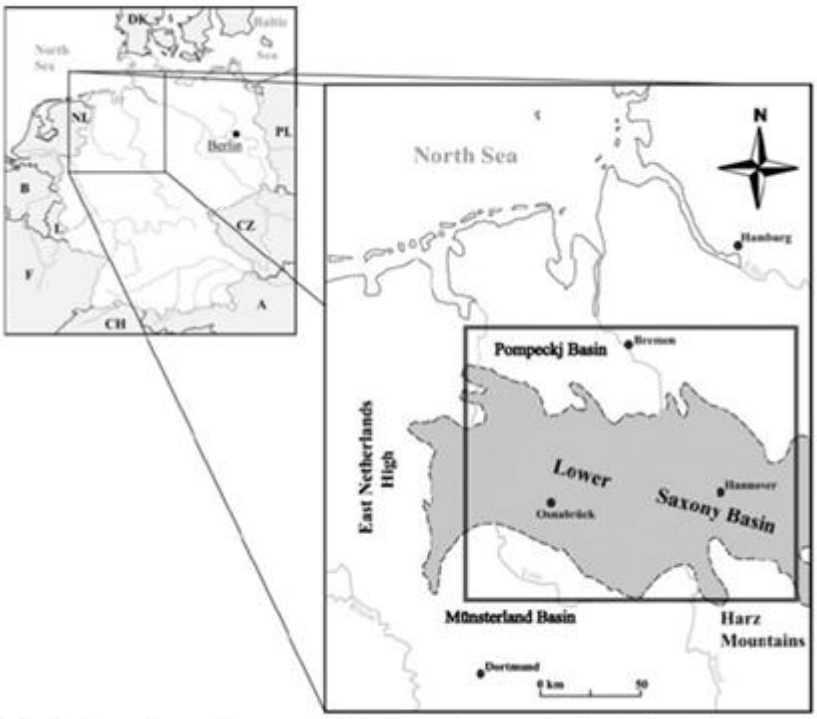

Fig. 1. Location and extent of the lower Saxony basin (after Rippen et al., 2013).

,

II. Petroleum geology of the lower Saxony Basin

Carboniferous coals

Stratigraphically, Carboniferous coal is the oldest and the first major source rock for gas generation in north western Germany. The coals have an average total organic carbon of 5%. During the lower Permian period volcanoclastic sediments were deposited which served as the main reservoir for the sequence. A structural trap was later formed that gave a room for vertical migration of hydrocarbon. Subsequently, a rock salt formation was accumulated which served as the seal due to the transition to shallow conditions that occurred during the Zechstein period. This led to the loss of generation potential to the early Westphalian coals at the end of middle Jurassic (Munoz, 2007). The Lower Saxony Basin is one of the oldest petroleum provinces with petroleum production dating from the 19th Century. Two important phases of compression, uplift and erosion (Variscan orogeny and Subhercynian inversion) affected sediments of the Lower Saxony Basin. These geological processes modified, created and destroyed porosity in sediments of the Lower Saxony Basin.

Posidonia shale

Posidonia shale, which was deposited during the lower Jurassic (Toarcian) period is the second major petroleum source rock in the lower Saxony Basin, it is located in the northern Germany covering 500sq km of the Hills syncline area. The Shale deposits are believed to be anoxic due to the fact that the formation is characterised by deep marine fossils (such as ammonites, sea lilies, schizopores, bivalves, coccolithopores) (Martill, 1993). Posidonia shale in the Hils Syncline is approximately 35m thick. The area exhibits a threefold stratigraphic subdivision: The upper calcareous shale, middle calcareous shales with bivalve shells and lower Marlstone. These units show minor differences in lithology. The marlstone unit and shale is distinguished by the carbonate content (Littke et al., 1991). The formation is almost entirely in the peak oil window which covers the basin except to the westernmost part.

Posidonia shale is organically rich and lateral variations in its maturity have been related to its deep burial or the effects of Vlotho Massif or professed deep seated igneous intrusion. (Horsfield et al., 2010). Although, a low rank of maturity gradient in the lower Saxony basin which suggest burial rather than an igneous intrusion (Munoz, 2007).

Wealden shale

The third main source rock is the Wealden shale formed during the lower cretaceous, found at the westernmost part of the lower Saxony basin. The younger Wealden shale, well known as Papershale of the

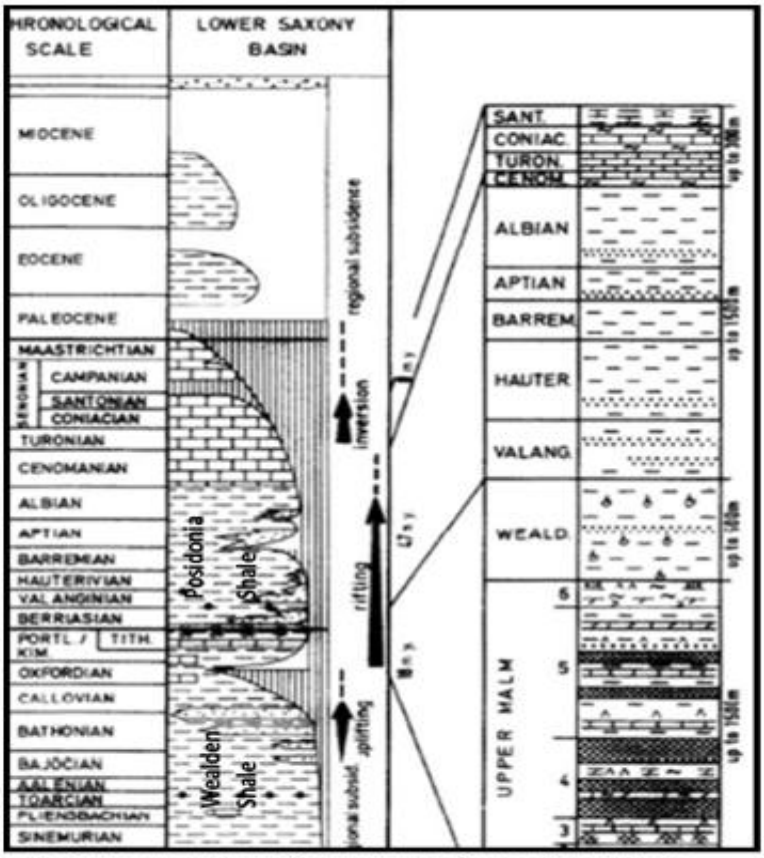

Fig. 2. Tectonostratigraphic Framework of Lower Saxony Basin. (modified from Scharzer and Littke, 2007).

Cretaceous age occurs only in western half of the basin. Wealden shale is brackish to limnic (rare overturn or eruption) in facies and contain high amounts of sedimentary organic matter with significant hydrocarbon potential. Munoz 2007 documented that the Wealden shale has total organic carbon up to 8%. This formation was overlain by deltaic sandstones and the upper Cretaceous shales served as reservoir and sandstones respectively. At the time the basin was inverted the centre of the basin was eroded. Although, recent studies have shown that the maturity of the outcropping Wealden basin centre had already entered the gas window even prior to the inversion episode. Maturity increases from the basin margins towards the basin centre (Munoz, 2007).

III. Material and methods

The Posidonia shale samples were collected from Schlahe well at the depth of 30.2m. The Wealden samples were collected from Wickensen well at the depth of 923.7m. Both samples are located in the lower Saxony basin of Germany. These samples were examined to simplify interpretation of pore network properties using FIB- SEM and BIB SEM techniques. Focused ion beam (FIB) and broad ion beam (BIB) together with scan electron microscope (SEM) were used. These involve using high resolution of gallium (Ga+) ion beam and argon (Ar+) ion beam respectively. It produces high resolution images which ease visual characterization of pore structures down to micron scale. Representative samples of both Posidonia and Wealden shales were characterized first by FIB-SEM, BIB SEM and mercury intrusion porosimetry (MIP). MIP was used for comparison of interpreted MIP pore size distributions and total porosity with that of the representative samples.

Samples were slowly air dried at room temperature at a relative humidity for one week. These samples were weighed before and after drying to estimate the water loss. Polishing of samples mechanically was employed on the samples embedded in a holder to achieve a flat cross section. FIB images were polished using an acceleration voltage of 30 kV. For BIB cross sections ultrasound cutter was used to cut the samples. These cross sections samples were pre-polished to reduce the roughness and smoothen flat to minimize curtaining effect and produce a better broad ion beam cross section (Desbois et al., 2011). This helps not only to smooth the edge of the sample but also to eliminate pre-polish damage attained during early polish preparation. This flat cross section allows the surface to be milled to a degree of smoothness which enables the assessment of classifying minerals, pore type and pore distribution across the entire surface.

Hitachi SU-70 High Resolution Analytical Scanning Electron Microscope, equipped with an Oxford Instrument Energy Dispersive X-ray microanalysis system (INCA Energy 700) was used. Operating conditions of the Schottky field emission gun was operated at an acceleration voltage of 15KV. The use of these techniques obviously produces very high quality cross section without damage to investigate the pore network of samples at high resolution. Backscatter electron (BSE) images were obtained using an yttrium-aluminum garnet (YAG) scintillator detector. Microanalysis settings for Energy-dispersive X-ray spectrometry (EDX) collection was conducted at process time 5, collection at 30sec and an acquisition rate of more 2.5K counts per second.

Apart from visual identification of minerals and pores, Jmicrovision 1.2.7 software was used to run the simulation of the FIB-SEM and BIB-SEM images. Quantification of pores was carried out by point counting method of the Jmicrovision software. The representative elementary area (REA) for the pores of both Posidonia and Wealden shale in a polished cross section and was determined on porosity using SE image, while BIB-SEM was used to identify and typify pores respectively.

Increase in size of the boxes increases the percentage of the area defined in terms of both mineralogy and porosity. REA allows the qualitative and quantitative study of structures and porosity. Kameda et al., 2006 documented that there is fluctuation of the measured mineralogy, porosity and pore size distribution of a larger area to a smaller area covered by the micrograph.

BIB images were extracted with object extraction tool using Jmicrovision computer software. The extraction of the binary images allows the differentiation of pores and fractures. Binary images of both Posidonia and Wealden samples were analysed and extracted. The tool eliminated fractures on each of the 30 images of both Posidonia and Wealden samples and pore properties were calculated.

Mercury intrusion porosimetry (MIP) is a method used for typifying the distribution of pore sizes in porous medium (Urai, 2003). The idea of this technique is to intrude mercury with sufficiently high pressure to invade the pore spaces. Washburn equation converts mercury pressure to pore throat diameter (Washburn, 1921). Small pore throat sizes are filled with mercury induced with high pressure. One gram each of both WIC 007129 for Posidonia and EX-A010305 for Wealden samples were used for the MIP experiment. Samples were freeze dried and oven dried at -500C and 80C for one week. These samples were placed in a pressure vessel in which pressure was introduced at 25Psi and slowly increased to 39,000Psi. This data was used for calculating total porosity and pore size distribution.

IV. Result

Porosity distribution and classification

Interparticle pores

Interparticle pores are pores between grains and crystal. Samples show characteristics of an angular shape pores which were observed to be clustered in one area (Fig. 3A.) which could probably inferred to the heterogeneity of the samples. Interparticle pores are dominantly elliptical pores connected by tube-like pore-throats observed in clay matrix at a high resolution of 1µm.

Several pores were identified but these pores are in nanometer scale, most of which were found within clay matrix, pyrite framboid and fossils. Based on Loucks et al., (2011) concept of pores classification, these pores were classified. Average values of both Posidonia and Wealden representative samples represented on ternary diagrams with peak end members as Organic matter pores, Interparticle pores and Intraparticle pores (Fig. 4).

Intraparticle pores

Intraparticle pores are pores within grains (Loucks et al., 2011). Interparticle pores observed in this study are mostly angular, irregular and/or ellipsoidal in shape but other morphologies are also present. Angular sections are the most common pore outline (Fig. 3B). Although, at higher resolution, many of these pore shapes tend to appear less angular and elliptical and they exhibit more drawn-out edges. Intraparticle pores identified in all the samples show interconnectivity. Intraparticle pores include the carbonate mineral dissolution pores (Fig. 3C and D).

Organic matter pore

Thermal maturity of mudstones and kerogen degradation during catagenesis are considered factors influencing the development of organic matter pores (Curtis et al., 2010). In both the samples examined, organic matter pores were not identified except for a few micropores observed along the rims of grains (Fig. 3B).

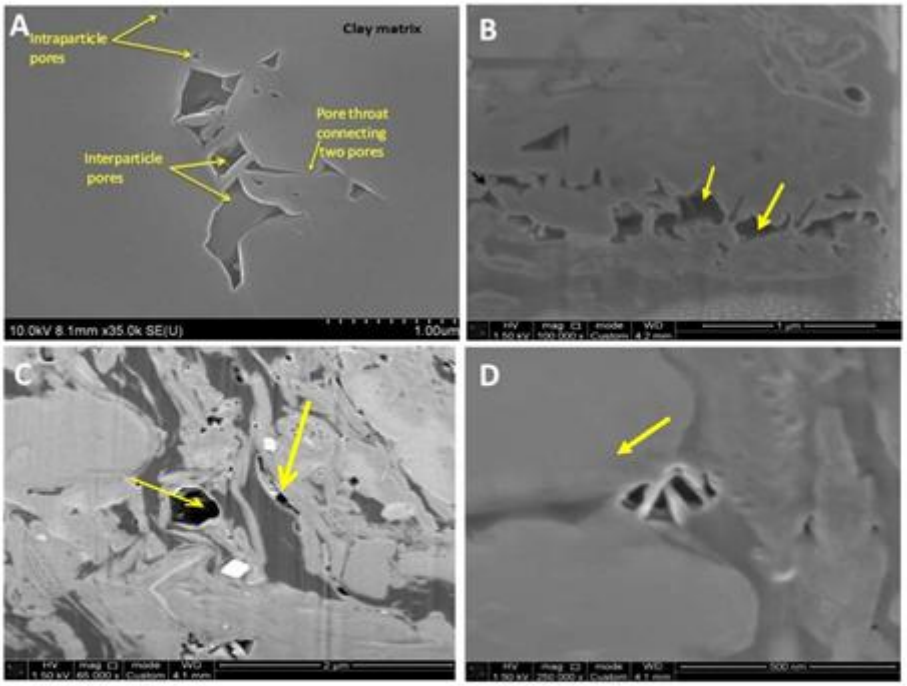

Fig. 3. Secondary electron SE image at high resolution showing types of pores in clay matrix. A, Interparticle pores and intraparticle pores connected with small pore throat, B, showing intraparticle pores formed by dissolution of rim around a mineral microrhomb with tube like (arrows) pore throat connecting. C, pores showing artefacts formed by beam interaction. Large pore at the centre of the image could be formed by dissolution of detrital minerals and D, dissolution of clay minerals. Arrow shows pore spaces in the studied sample.

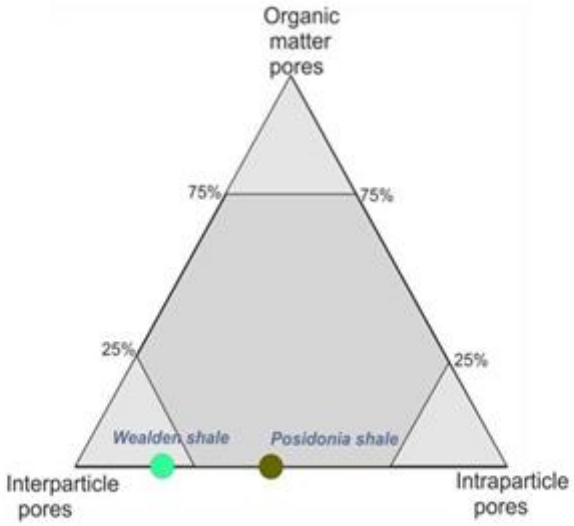

Fig. 4. Ternary diagram reveals the percentage of pores of Posidonia and Wealden shales.

Pore statistics

The use of high resolution SEM imaging in combination with (Ga+) ion beam and (Ar+) ion beam enables the identification of microstructures in 2D cross-sections. This high quality cross-sections rendered not only qualitative but also statistical interpretation of pores. Simple geometry related to bulk porosity was

employed to estimate these porosities. Total porosity of both Posidonia and Wealden shale was estimated using the sum of individual pore areas by that of the image width and height. This could be well illustrated below:
Porosity of Posidonia samples are calculated as thus:
Porosity = Σ Area / Image width x Image height x No of images
= 89917075.09/ 12761.088 x 9570.816 x 30
= 0.0245405471 x 100
= 2.5 %
Porosity of Wealden samples are calculated as thus:
Porosity = Σ Area / Image width x Height of image x No of images
= 18818147.75/ 12761.088 x 9570.816 x 30
= $5.135928329 \times 10^{-3}$ x100
= 0.52%
However, differentiating pores and fractures were not easy. This study used the same approach to estimate the porosity of fractures. Fracture porosity of both shaly facies are calculated below.
Fracture porosity for Posidonia shale is estimated thus:
Fracture porosity = Σ Area / Image width x Height of image x No of images
= 1552728953.2/3664020756
= 0.04168343014 x 100
= 4.2 %
Fracture porosity for Wealden shale is calculated thus:
Fracture porosity = Σ Area / Image width x Height of image x No of images
= 59655827/3664020756
= 0.01628151994 x100
= 1.63%

Mercury porosimetry

30 samples from WIC 007129 and EX-A 010305 wells of Posidonia and Wealden shales were intruded with mercury. Volumes of WIC 007129 and EX-A 010305 samples used for this purpose were 0.49cm3 and 0.71cm3 respectively. Before the experiment the weights of the samples were 138.4256 and 133.0380 grams in WIC 007129 and EX-A 010305 respectively. Volumes of mercury used for the penetration were 6.0544 and 5.8467 in that order. Mercury pressure was converted to pore throat diameter using the Washburn equation (Washburn, 1921). Mercury porosity was estimated based on the difference between the maximum and the minimum pore detected by mercury. This is shown below:
Mercury (Hg) porosity: Maximum pore – Minimum pore x 100
For Posidonia shale = 0.0959846 – 0.033923
= 0.0620616 x 100
= 6.2%
For Wealden shale = 0.0136899 – 0.0438422
= 0.0598477 x 100
= 5.9%
Percentage of total connected porosity intruded by mercury was also calculated using the same approach where the difference between the maximum and the minimum pore viewed is divided by total porosity of mercury. This is illustrated below:
For Posidonia:
Percentage of pores = Pore difference –total porosity
= (0.0959846 – 0.033923) / 0.105061
= 0.5907196771 x 100
= 59%
For Wealden:
Percentage of pores = Pore difference –total porosity
= (0.1036899 – 0.0438422)/ 0.143018
= 0.418462711 x 100
= 41%

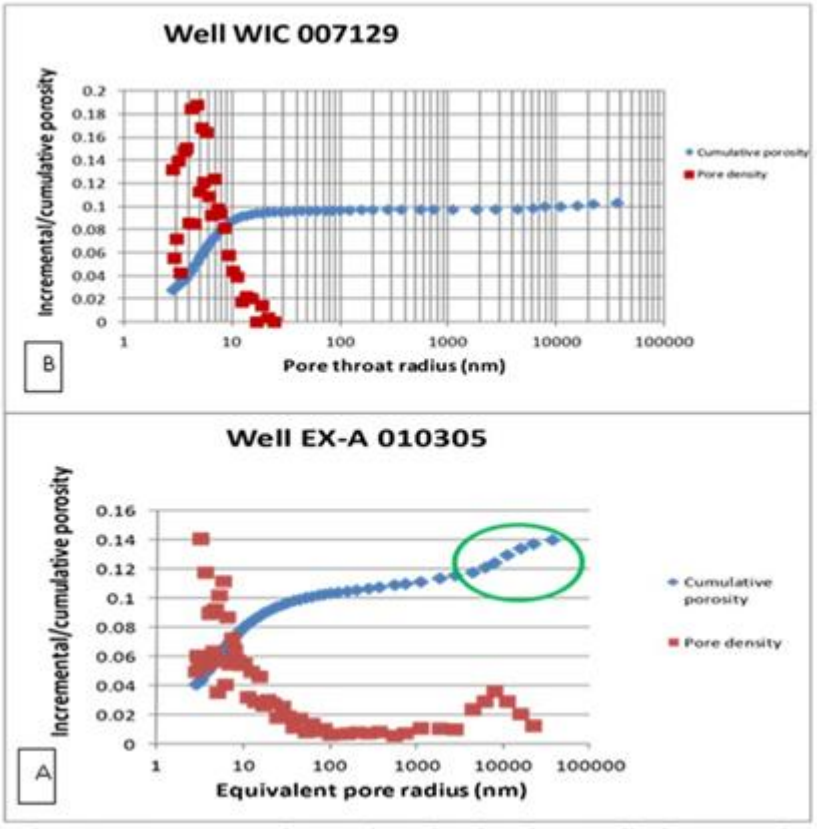

Fig. 5: Mercury porosimetry data showing the contribution to total porosity vs. pore throat radius for A. Wealden and B. Posidonia samples.

Table no 1. Measured porosities of Posidonia and Wealden Shales

Sample	**Posidonia**	**Wealden**
Total porosity TP (%)	2.5	0.5
Mercury Porosity Hg P (%)	6.2	5.9
Total pores connected by Hg (%)	59	41
Fracture porosity FP (%)	4.2	1.63

V. Discussion

Pore types, geometry and origin

Pores identified in the studied samples were mainly found within clay matrix with little contribution from pyrite framboid and fossils. Quartz and calcite are considered non-porous minerals. These nanopores could be primary (i.e. formed during thermal maturation of hydrocarbon) or secondary pores formed during dissolution of carbonates minerals. Pores are formed during thermal maturation when Kerogen is converted to hydrocarbon leading in the formation of liquids and gases (Loucks et al., 2009). Also during thermal maturation surface area of shale increases as the percentage of micropores increases (Hua et al., 2011). Most pores found within the clay matrix are significantly small and elongate while pores found within pyrite crystals and fossils are much smaller than the pores in clay matrix. Interparticle pores show predominantly angular to elliptical shape pores. These elliptical pores at high resolution show tube like pore throat connecting them.

Intraparticle pores appear less angular and ellipsoidal in shape; other pore morphologies also exist as shown in (Fig. 3B). These pores also appear along rims of grains (Fig. 3B). Intraparticle pores are less abundant between pyrite crystals. Slatt and O'Brien (2011) documented that intraparticle pores in pyrite crystal grains which are dispersed within shale matrix could probably reduce permeability. In both study samples observed intraparticle pore show no connectivity. Interparticle pores have the highest percentage in occurrence than intraparticle pores in both Posidonia and Wealden shale (Fig. 9). Both Posidonia and Wealden shales are dominated by interparticle pores (i.e. pores between particles). No organic matter pore found in both study samples.

Pore types are not in abundance due to the heterogeneity of the samples and lack of pore formation in organic matter could be associated with maturity. Representative elementary areas of both study sample (Fig. 7 and 8) show porosity at a minimum area 80 x 80 μm^2 to be representative.

Crack formation

Cracks in clay rich formations are formed due to stress release. Drying of samples involves several mechanisms each of which can induce cracks, either air dried, oven dried or freeze dried. Shale has the property of shrinkage when water is dried exuded. The effects of drying on mudrocks have been documented in literature e.g. (Soe et al., 2009; Holzer et al., 2010; Simms and Yan Ful, 2001). This study freeze dried samples for MIP at -50^0C for one week and oven dried at 8^0C for one week. Freeze and oven drying of samples involve high pressure which probably leads to the formation of cracks. Clearly visible cracks with rough edges and sharp thin tips at both ends and deeper than the depth focus have been observed. The morphology of the cracks observed in this study is most likely to have been induced by hydration of stress during mercury injection porosimetry experiment. This indicates that they were not primarily formed and may be related to relaxation stress (Desbois, 2012) or due to compaction (Chester et al., 2004). However if these cracks are formed due to either of the reasons mentioned above then measurement of mercury porosimetry should be revisited to get the accurate porosity of the samples.

Pore connectivity

To understand the fluid flow of a system, it is necessary to identify the connectivity of pores. Although, it is difficult to visually observe pore connectivity. Mercury intrusion porosimetry experiments revealed that pores were connected giving the value of 6.2 % and 5.9 % for WIC 007129 (Posidonia) and EX-A010305 (Wealden) respectively. This study observed poor connectivity in fossil, pyrite framboid and crack regions to the clay matrix for both Posidonia and Wealden samples. However, interparticle pores in clay matrix seem to be connected, but this connectivity of pores is in nanometer scale. From MIP experiment the percentage of total pores connected by mercury are 59% and 41% for Posidonia and Wealden shales respectively. The poor connectivity of pores in this study could be as a result of the immature state of the sample.

Variation of measured and mercury porosities

Total porosity measured for both samples is 2.5% and 0.5% for Posidonia and Wealden shales respectively. The porosity percentages are not in agreement with the measured porosity from mercury data which gives higher values of 6.2% and 5.9% of Posidonia and Wealden shales in that order. Although, mercury injection porosimetry (MIP) was able to recognize pores smaller than 3nm which could not have been seen visually. Fracture porosity in this study has also been determined were pores are extracted from cracks. This gave percentage values of 4.2% and 1.6% of Posidonia and Wealden shales respectively. The comparison of all measured porosities is summarized in (Table 1).

VI. Conclusion

Pore types found in both Posidonia and Wealden samples are predominantly interparticle pores, with little connectivity and intraparticle with no connectivity. And lack of organic matter could be related to the immature state of the samples. The presence of illite-smectite mineral in both samples may probably hinder permeability. Both samples show low porosity. From the above mentioned values this study concludes that mercury porosity did not only calculate actual pores but in combination with fractures or cracks. Mercury porosity could not be true considering the depth and immature state of the samples. However, the limitation of FIB-SEM and BIB-SEM technique include the formation of artefacts due to beam interaction.

Reference

[1]. Chester, J. C., Lenz, S. C., Chester, F. M. and Lang, R. (2004) Mechanisms of compaction of quartz sand at diagenetic conditions. Earth and Planetary Science Letters, **220**, 435-451.

[2]. Curtis, M., Ambrose, R. and Sondergeld, C. (2010) Structural characterisation of gas shales on the micro and nono-scales. SPE, 15p.

[3]. Debois, G., Urai, J. L., Kukla, P. A., Konstanty, J. and Baerle, C. (2011) High resolution 3D fabric and porosity model in a tight gas reservoir: A new approach to investigate microstructures from mm-to-mm scale combining argon beam, cross-sectioning and SEM imaging. Journal of Petroleum Science and Engineering, **78**, 2, 243-257.

[4]. Gareth R. Chalmers, R. Marc Bustin, and Ian M. Power (2011) Characterization of gas shale pore systems by porosimetry, pycnometry, surface area, and field emission scanning electron microscopy/transmission electron microscopy image analyses: Examples from the Barnett, Woodford, Haynesville, Marcellus,and Doig units. American Association of Petroleum Geologists Bulletin **96,** 6, 1099-1119.

[5]. Holtzer, L., Munch, B., Rizzi, M. Wepf, R., Marshall, P. and Graulet, T. (2010) 3D-Microstructure analysis of hydrated bentonite with cryo-stabilized pore water. Applied Cay Science, **47**, (3/4), 330-342.

[6]. Holtzer, L., Indutnyi, F., Gasser, P.Munch, B. and Wegmann, M. (2007) Three-dimensional analysis of porous $BaTiO_3$ ceramic using FBI Nano tomography. Journal of Microscopy, **216**, 84-95.]

[7]. Horsefield, B., Littke, R., Mann, U. Bernard, S., L., Ulrichman, S. B., Tiemanh, T. V., Rawland, D. and Hans-martin, (2010) Shale gas in the Posidonia shale Hils area, Germany. American Association of Petroleum Geologists Annual Convention, New Orleans, LA, 11-14.]
[8]. Kameda, A., Dvorkin, J., Keehm, Y., Nur, A. and Bosi, W. (2006) Permeability-porosity transforms from small sandstone fragments. Geophysics, **71**, N11-N19.
[9]. Littke, R., Klussmann, U., Kroos, B. and Leythaeuser, D. (1991) Quantification of loss of calcite, pyrite and organic matter due to weathering of Toarcian black shales and effects on kerogen and bitumen characteristics. Geochemica et Cosmochemica Acta, **55**, 3369-3378.
[10]. Littke, R., Leythaeuser, D., Rullkotter, J. and Baker, D. (1991) Keys to the depositional history of the Posdonia Shale (Toarcian) in the Hils Syncline, northern Germany. Geological Society of London, Special Publications, **58**, 311-333.
[11]. Loucks, G. Robert, R. M. R., Stephen, C. R. and Jarvie, D. M. (2009) Morphology, genesis and distribution of nanometre scale pores in siliceous mudstones of the Mississippian Barnet Shale. Journal of Sedimentary Research, **79**, 848-861
[12]. Loucks, R. G., S. Ruppel, R.M. Reed, and U. Hammes, (2011) Origin and classification of pores in mudstones from shale-gas systems: American Association of Petroleum Geologists, Search and Discovery article 40855.
[13]. Martill, D.M. (1993) Soupy Substrates: A Medium for the Exceptional Preservation of Ichthyosaurs of the Posidonia Shale (Lower Jurassic) of Germany. Kaupia – Darmstädter Beiträge zur Naturgeschichte, 2, 77-97.
[14]. Munoz, A. Y. (2007) The thermal history of the western Lower Saxony basin. Diese Dissertation ist auf den Internetseiten der Hochschulbibliothek online verfügbar. 134pp.
[15]. Reed, R. M. and Loucks, R. G. (2007) Imaging nanoscale pores in the Mississippian Barnett Shale of the northern Fort Worth Basin (abs.): American Association of Petroleum Geologists Annual Convention Abstracts, v. 16.
[16]. Rippen, D., Littke, R., Bruns, B. and Mahlstedt, N. (2013) Organic geochemistry and petrography of Lower Cretaceous Wealden black shales of the Lower Saxony Basin: The transition from lacustrine oil shales to gas shales. Organic Geochemistry, **63**, 18–36.
[17]. Simms, P. H. and Yanful, E. K. (2001) Measurement and estimation of pore shrinkage and pore distribution in a clayey till during soil-water characteristic curve tests. Canadian Geotechnical Journal, **38**, 741-754.
[18]. Slatt, R. M. and O'Brien, N. R. (2011) Pore types in the Barnett and Woodford gas shales: Contribution to understanding gas storage and migration pathways in fine-grained rocks. American Association of Petroleum Geologists Bulletin, **95**, (12), 2017-2030.
[19]. [19] Soe, A. K. K., Osada, M., Takahashi, M. and Sasaki, T. (2009) Characterization of drying-induced deformation behaviour of Opalinus Clay and tuff in no-stress regime. Environmental Geology, **58**, 1215-1225.
[20]. Sondergeld, C. H., Ambrose, R. J., Rai, C. S. and Moncrieff, J. (2010) Microstructural studies of gas shale: Society of Petroleum Engineers unconventional Gas Conference, Pittsburgh, Pennsylvania. SPE Paper 131771, 17.
[21]. Urai, J. L. (2003) Microstructural evolution and grain boundary structure during static recrystallization in synthetic polycrystals of sodium chloride containing saturated brine. In: AGU Fall 2003. AGU, Sam Francisco, USA (poster presentation).
[22]. Washburn, E. W. (1921) Note on a method of determining the distribution of pore sizes in a porous material. Proceeding of the National Academy of Sciences of the United States of America, 7, 115.

IOSR Journal of Applied Geology and Geophysics (IOSR-JAGG) is UGC approved Journal with Sl. No. 5021, Journal no. 49115.

M. Bukar "Pore Systems Analysis of Posidonia and Wealden Shale's of Lower Saxony Basin, Germany." IOSR Journal of Applied Geology and Geophysics (IOSR-JAGG) 6.3 (2018): 09-17